UbiB proteins regulate cellular CoQ distribution

Zachary A. Kemmerer[1,2,7], Kyle P. Robinson[1,2,7], Jonathan M. Schmitz[1,2], Brett R. Paulson[4], Adam Jochem[1,2], Paul D. Hutchins[4], & Joshua J. Coon[3,4,5], and David J. Pagliarini[1,2,6*]

[1]Morgridge Institute for Research, Madison, WI 53715, USA.
[2]Department of Biochemistry, University of Wisconsin-Madison, Madison, WI 53706, USA.
[3]Genome Center of Wisconsin, Madison, Wisconsin 53706, USA.
[4]Department of Chemistry, University of Wisconsin-Madison, Madison, WI 53706, USA.
[5]Department of Biomolecular Chemistry, University of Wisconsin-Madison, Madison, WI 53706, USA.
[6]Departments of Cell Biology and Physiology; Biochemistry and Molecular Biophysics; and Genetics, Washington University School of Medicine, St. Louis, MO 63110
[7]These authors contributed equally to this work.
*e-mail: pagliarini@wustl.edu

Abstract

Coenzyme Q (CoQ, ubiquinone) is a redox-active lipid essential for many core metabolic processes in mitochondria, including oxidative phosphorylation[1-3]. While lesser appreciated, CoQ also serves as a key membrane-embedded antioxidant throughout the cell[4]. However, how CoQ is mobilized from its site of synthesis on the inner mitochondrial membrane to other sites of action remains a longstanding mystery. Here, using a combination of yeast genetics, biochemical fractionation, and lipid profiling, we identify two highly conserved but poorly characterized mitochondrial proteins, Ypl109c (Cqd1) and Ylr253w (Cqd2), that reciprocally regulate this process. Loss of Cqd1 skews cellular CoQ distribution away from mitochondria, resulting in markedly enhanced resistance to oxidative stress caused by exogenous polyunsaturated fatty acids (PUFAs), whereas loss of Cqd2 promotes the opposite effects. The activities of both proteins rely on their atypical kinase/ATPase domains, which they share with Coq8—an essential auxiliary protein for CoQ biosynthesis. Overall, our results reveal new protein machinery central to CoQ trafficking in yeast and lend new insights into the broader interplay between mitochondrial and cellular processes.

Extramitochondrial CoQ combats oxidative stress

To our knowledge, no proteins have yet been directly associated with cellular CoQ trafficking from mitochondria, but the extreme hydrophobicity of CoQ suggests that this process likely requires dedicated machinery. We sought to identify such proteins by exploiting CoQ's extramitochondrial antioxidant role. Budding yeast (*Saccharomyces cerevisiae*) lacking CoQ or phospholipid hydroperoxide glutathione peroxidases (PHGPx) are sensitive to the oxidative stress conferred by exogenous polyunsaturated fatty acids (PUFAs), such as linolenic acid (18:3)[5,6]. To force cells into relying more heavily on the antioxidant properties of CoQ, we deleted all three PHGPx genes in W303 *S. cerevisiae* (Δ*gpx1*Δ*gpx2*Δ*gpx3,* hereafter referred to as Δ*gpx1/2/3*). We validated that this strain is sensitized to 18:3 treatment and demonstrated that this sensitivity is dampened when cellular CoQ levels are augmented through supplementation with the soluble CoQ precursor 4-hydroxybenzoate (4-HB) (Fig. 1a-b). Importantly, the CoQ analog decylubiquinone was markedly more effective at protecting against PUFA stress than its mitochondria-targeted counterpart, mitoquinone,

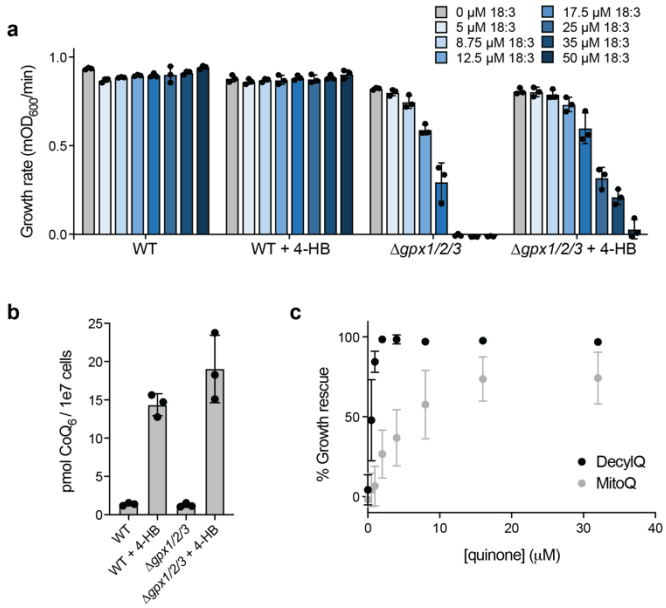

Fig. 1: Extramitochondrial CoQ combats oxidative stress. a, Growth rate of wild type (WT) and Δ*gpx1/2/3* yeast in synthetic complete media minus para-aminobenzoate (*p*ABA–) containing 2% (w/v) glucose (mean ± SD, n = 3) and the indicated additives. 4-hydroxybenzoate, 4-HB; linolenic acid (PUFA), 18:3. **b**, Total CoQ from WT and Δ*gpx1/2/3* yeast described in **a** (mean ± SD, n = 3). **c**, Rescue assay under the conditions described in **a** comparing the ability of decylubiquinone (DecylQ) and mitoquinone (MitoQ) to restore growth of Δ*gpx1/2/3* yeast treated with 35 μM 18:3 (mean ± SD, n = 3).

suggesting that extramitochondrial CoQ is the predominant mediator of PUFA resistance (Fig. 1c). This is consistent with previous data showing that exogenous PUFAs are incorporated into endogenous membranes slowly, and therefore, populate non-mitochondrial membranes first[6]. Thus, we established a strain whose survival in the presence of PUFAs is especially dependent on extramitochondrial CoQ.

Loss of Cqd1 confers PUFA resistance

We reasoned that suppressor mutations that increase extramitochondrial CoQ levels would enhance PUFA resistance in the Δ*gpx1/2/3* strain, so we performed a forward-genetic suppressor screen (Fig. 2a). We randomly mutagenized this strain with ethyl methanesulfonate (EMS) and isolated colonies tolerant of 18:3 treatment. From ~20,000 unique mutant colonies, we obtained four hit strains with substantial PUFA resistance (Fig. 2b). We then performed whole-genome sequencing that revealed non-synonymous mutations in 442 unique genes across these four strains (Extended Data Table 1). These mutants were ranked using PROVEAN (Protein Variation Effect Analyzer), a software tool for predicting deleterious protein changes[7]. PROVEAN assigns a disruption score (D-Score) that reflects the likelihood that a given mutation is deleterious. In our collective dataset, 99 genes achieved a D-Score below the strict threshold of -4.1 (Fig. 2c; Extended Data Table 1). Given the overall limited overlap in hits between mutant strains, it is likely that our dataset includes multiple genes that contribute to an enhanced PUFA resistance phenotype.

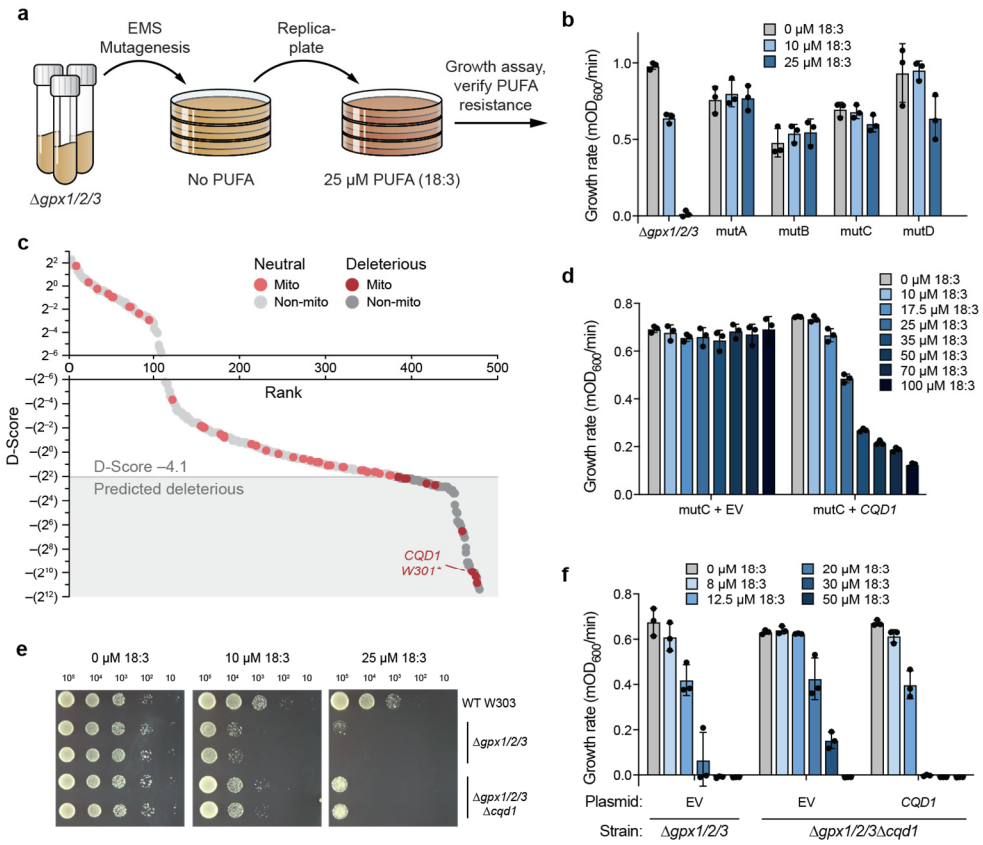

Fig. 2: Genome-wide screen for CoQ trafficking genes identifies uncharacterized UbiB protein Cqd1. **a**, Schematic of forward-genetic yeast screen for genes involved in CoQ trafficking. **b**, Growth rates of Δ*gpx1/2/3* and four mutant strains resistant to 18:3 treatment (mutA-D). Yeast were assayed in *p*ABA– media containing 2% (w/v) glucose with 0-25 μM 18:3 (mean ± SD, n = 3). **c**, Mutant strains mutA-D were submitted for whole-genome sequencing to identify non-synonymous mutations (total = 442). Mutations were analyzed with PROVEAN to filter for likely deleterious changes (D-score ≤ -4.1, shaded box). Gray, all genes; red, mitochondrial genes. Light, predicted neutral; dark, predicted deleterious. **d**, Growth rate of mutC yeast expressing empty vector (EV) or endogenous *CQD1* (mean ± SD, n = 3). Yeast were assayed under the conditions described in **b** with 0-100 μM 18:3. **e,** Drop assay of WT, Δ*gpx1/2/3*, and Δ*gpx1/2/3*Δ*cqd1* yeast grown for 3 days on solid *p*ABA– medium containing 2% (w/v) glucose, 0.5% (w/v) ethanol (EtOH), and 0-25 μM 18:3. **f**, Growth rates of Δ*gpx1/2/3* and Δ*gpx1/2/3*Δ*cqd1* yeast expressing EV or endogenous *CQD1* (mean ± SD, n = 3). Yeast were assayed under the conditions described in **b** with 0-50 μM 18:3. Source data for panel **c** is provided as a Source Data file.

We chose to focus on mitochondrial proteins for further examination since, to our knowledge, trafficking machinery at the site of CoQ synthesis in mitochondria has yet to be identified. Of the nine mitochondrial proteins harboring likely deleterious mutations, one, Ypl109c (renamed here as Cqd1, see below), is an uncharacterized protein that resides on the inner mitochondrial membrane (IMM), making it an attractive candidate for further study (Fig. 2c; Extended Data Fig. 1a). Moreover, Cqd1 possesses the same

UbiB family atypical kinase/ATPase domain as Coq8, an essential protein for CoQ synthesis that resides on the matrix face of the IMM[8-11]. Our recent work suggests that Coq8 ATPase activity may be coupled to the extraction of hydrophobic CoQ precursors from the IMM for subsequent processing by membrane-associated matrix enzymes[12]. Cqd1 resides on the opposite side of the IMM, facing the intermembrane space[9,13] (Extended Data Fig. 1b), physically separated from the other CoQ-related enzymes but still positioned for direct access to membrane-embedded CoQ precursors and mature CoQ. Furthermore, a recent study reported that haploinsufficiency of human *CQD1* ortholog *ADCK2* led to aberrant mitochondrial lipid oxidation and myopathy associated with CoQ deficiency[14].

In our screen, mutant C (mutC) contains an early stop codon in *CQD1* (Fig. 2c, Extended Data Fig. 1c). To test whether this mutation is important for mutC's phenotype, we reintroduced WT *CQD1* into this strain under its endogenous promoter. Indeed, this reintroduction re-conferred PUFA sensitivity (Fig. 2d). Furthermore, deletion of *CQD1* in the parent Δ*gpx1/2/3* strain, which lacks all other mutC mutations, was sufficient to enhance PUFA resistance (Fig. 2e-f). Collectively, these data demonstrate that disruption of *CQD1* is at least partially causative for mutC's PUFA-resistant phenotype.

Cqd1 affects CoQ distribution

Our results above suggest that loss of *CQD1* confers cellular resistance to PUFA-mediated oxidative stress by increasing extramitochondrial CoQ. We reasoned that this was likely rooted either in a general increase in CoQ production or in its redistribution. To test these models, we first measured total levels of CoQ and its early mitochondrial

precursor polyprenyl-4-hydroxybenzoate (PPHB) in cells lacking *CQD1* or control genes (Fig. 3a-c). As expected, disruption of *HFD1*, which encodes the enzyme that produces the soluble CoQ precursor 4-HB, led to loss of CoQ and PPHB, while disruption of *COQ8* caused complete loss of CoQ with the expected buildup of the PPHB precursor. However, we found no significant change in CoQ or PPHB levels in the Δ*cqd1* strain, demonstrating that Cqd1 is essential neither for CoQ biosynthesis nor the import of CoQ precursors under the conditions of our analyses.

To next examine CoQ distribution, we fractionated yeast and measured CoQ levels (Fig. 3d; Extended Data Fig. 2a). We observed that Δ*cqd1* yeast had a significant increase in CoQ from the non-mitochondrial (NM) fraction, consisting of organelles and membranes that do not pellet with mitochondria, and a corresponding decrease in mitochondrial (M) CoQ. Deletion of the tricarboxylic acid (TCA) cycle enzyme Kgd1 had no effect on relative CoQ levels (Fig. 3d) despite causing a deficiency in respiratory growth (Fig. 3e), indicating that general mitochondrial dysfunction does not perturb CoQ distribution. The increased extramitochondrial CoQ in Δ*cqd1* yeast is consistent with the observation that deleting *CQD1* increases PUFA resistance (Fig. 2e-f).

To our knowledge, this is the first example of a genetic disruption leading to altered cellular distribution of endogenous CoQ, hence our renaming of this gene CoQ Distribution 1 (*CQD1*). To further validate this finding, we examined growth in glycerol, a non-fermentable carbon source, which requires an intact mitochondrial electron transport chain. We reasoned that a decrease in mitochondrial CoQ would disrupt respiratory growth in media depleted of CoQ precursors. Indeed, deletion of *CQD1* significantly reduced respiratory growth rate in this medium (Fig. 3e). To confirm that

this defect is caused by CoQ depletion, we rescued growth with CoQ of different isoprene tail lengths (CoQ_2 and CoQ_4) and with CoQ precursors, which are more readily delivered due to their solubility (Fig. 3f). Endogenous expression of *CQD1* rescued respiratory growth without affecting total CoQ levels (Fig. 3g, Extended Data Fig. 2b), further supporting the hypothesis that CoQ distribution, not biosynthesis, is perturbed in Δ*cqd1* yeast.

We next sought to begin understanding how Cqd1 functions in CoQ distribution. Our recent work on Cqd1's UbiB homolog COQ8 (yeast Coq8 and human/mouse

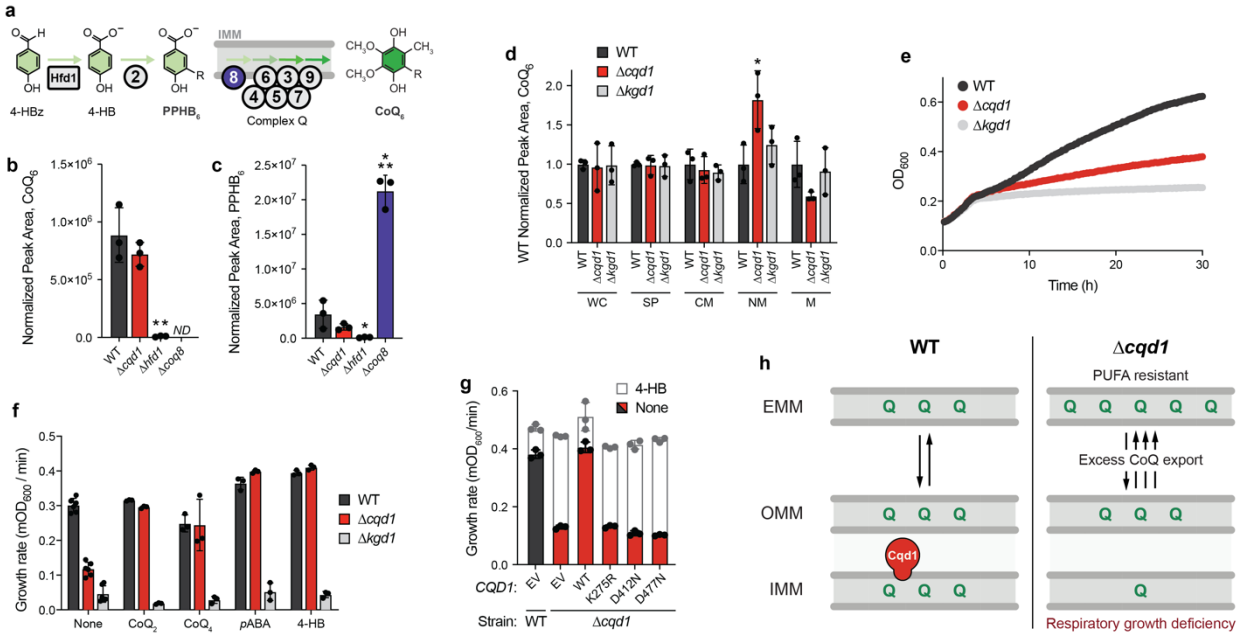

Fig. 3: Cqd1 influences cellular CoQ distribution. a, Schematic of CoQ biosynthesis pathway. Polyprenyl hydroxybenzoate (PPHB) is an early precursor that undergoes a series of head group modifications by IMM-associated Coq enzymes (complex Q) to produce CoQ. Hfd1 is essential for PPHB synthesis, while Coq8 is required for production of CoQ. **b**, Total CoQ and **c**, polyprenyl-4-hydroxybenzoate (PPHB) from WT, Δ*cqd1*, Δ*hfd1*, and Δ*coq8* yeast (mean ± SD, n = 3); not detected, ND. **d**, CoQ from subcellular fractions derived from WT, Δ*cqd1*, and Δ*kgd1* yeast (mean ± SD, n = 3). Spheroplast, SP; crude mitochondria, CM; non-mitochondrial fraction, NM; enriched mitochondria, M. **e**, Growth assay of WT, Δ*cqd1*, and Δ*kgd1* yeast in *p*ABA– media containing 0.1% (w/v) glucose and 3% (w/v) glycerol (mean, n = 6). Yeast enter the respiratory phase of growth after ~4 hours in this growth condition. **f**, Growth rate of WT, Δ*cqd1*, and Δ*kgd1* yeast assayed under conditions described in d (mean ± SD; none n = 6, all others n = 3). Yeast were grown in the presence and absence of 100 μM CoQ analogs (CoQ_2, CoQ_4) and 1 μM CoQ precursors (*p*ABA, 4-HB). **g**, Growth rate of WT and Δ*cqd1* yeast transformed with the indicated plasmids (EV, *CQD1* or *CQD1* point mutants) and grown in Ura–, *p*ABA– media containing 0.1% (w/v) glucose and 3% (w/v) glycerol (mean ± SD, n = 3). Yeast were treated with 0 (colored bars) or 1 μM 4-HB (white bars, superimposed) to determine rescue of respiratory growth. **h**, Model for Cqd1's putative role in cellular CoQ distribution. Significance calculated by a two-tailed Student's *t*-test; * = $p < 0.05$, ** = $p < 0.01$, *** = $p < 0.001$.

COQ8A) revealed that it possesses an atypical protein kinase-like (PKL) fold that endows ATPase activity but occludes larger proteinaceous substrates from entering the active site[11,15] (Extended Data Fig. 2c-e). Unlike COQ8, Cqd1 is recalcitrant to recombinant protein purification; therefore, in lieu of direct in vitro activity assays, we examined the ability of Cqd1 point mutants to rescue the respiratory growth defect of Δ*cqd1* yeast. Similar to Coq8[11,12,15], the ability of Cqd1 to rescue the Δ*cqd1* respiratory growth deficiency depended on core protein kinase-like (PKL) family residues[16] required for phosphoryl transfer (Fig. 3g) and on quintessential UbiB motif residues (Extended Data Fig. 2e-h). Further biochemical work is required to prove Cqd1's enzymatic activity; however, these data support a model whereby Cqd1's ability to promote CoQ distribution relies on atypical kinase/ATPase activity (Fig. 3h).

Cqd2 counteracts Cqd1 function

Beyond Coq8 and Cqd1, the *S. cerevisiae* genome encodes just one other member of the UbiB family—Ylr253w (aka Mcp2, and renamed here Cqd2). Cqd2 is also poorly characterized and resides in the same location as Cqd1, on the outer face of the IMM[9,13,17] (Extended Data Fig. 1b). Previous studies have identified genetic and physical interactions connecting Cqd2 to mitochondrial lipid homeostasis, but not to a specific pathway[17-19]. Given the similarity between these three proteins (Extended Data Fig. 2d-e), we anticipated that Cqd2 might also be connected to CoQ biology.

To test this hypothesis, we disrupted *CQD2* in Δ*gpx1/2/3* yeast and subjected this strain to PUFA-mediated stress. Surprisingly, Δ*gpx1/2/3*Δ*cqd2* yeast exhibited an enhanced sensitivity to PUFA treatment—the opposite phenotype to that of Δ*gpx1/2/3*Δ*cqd1* (Fig. 4a; Extended Data Fig. 3a). Furthermore, Δ*gpx1/2/3*Δ*cqd1*Δ*cqd2*

154 yeast phenocopied the parental (Δ*gpx1/2/3*) strain (Fig. 4a; Extended Data Fig. 3a).

155 Under respiratory conditions, Δ*cqd2* yeast exhibited no detectable change in growth.

156 However, deleting *CQD2* from Δ*cqd1* yeast (Δ*cqd1*Δ*cqd2*) restored this strain's impaired

157 respiratory growth rate to WT levels (Fig. 4b-c). Conversely, reintroduction of *CQD2* into

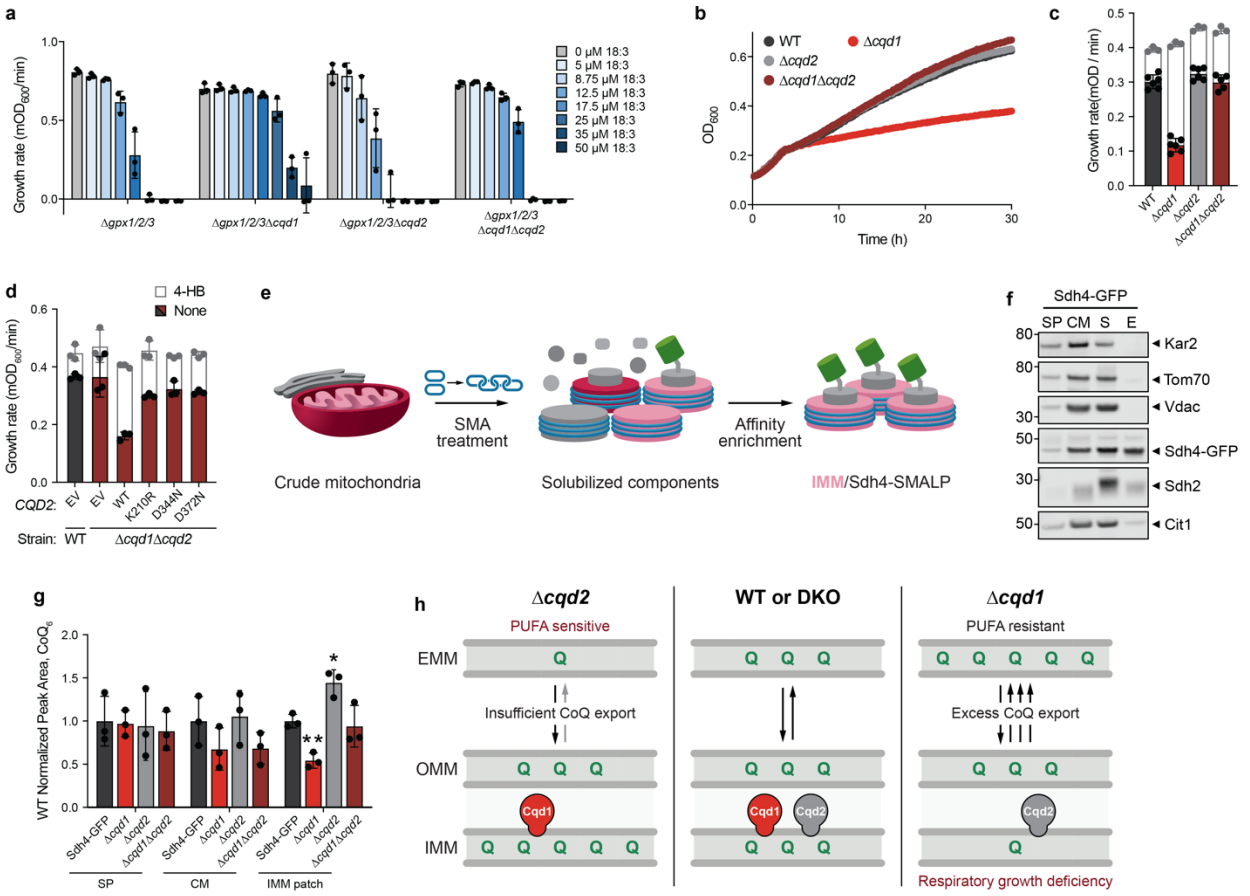

Fig. 4: Cqd2 function opposes Cqd1 control of CoQ distribution. a, Growth rate of Δ*gpx1/2/3* and the described yeast strains in *p*ABA– media containing 2% (w/v) glucose and the indicated additives (mean ± SD, n = 3). **b**, Growth assay of WT, Δ*cqd1*, Δ*cqd2*, and Δ*cqd1*Δ*cqd2* yeast in *p*ABA– media containing 0.1% (w/v) glucose and 3% (w/v) glycerol (mean ± SD, n = 6). **c**, Growth rate of yeast strains in b treated with 0 (colored bars) or 1 μM 4-HB (white bars, superimposed) (mean ± SD; 0 μM 4-HB n = 6, 1 μM 4-HB n = 3). **d,** Growth rate of WT and Δ*cqd1*Δ*cqd2* yeast transformed with the indicated plasmids (EV, *CQD2* or *CQD2* point mutants) and grown in Ura–, pABA– media containing 0.1% (w/v) glucose and 3% (w/v) glycerol (mean ± SD, n = 3). Yeast were treated with 0 (colored bars) or 1 μM 4-HB (white bars, superimposed) to determine recapitulation of respiratory growth defect. **e**, Schematic of Sdh4-GFP styrene maleic acid (SMA) lipid particle (SMALP) isolation. **f**, Western blot to assess purity of SMALP isolation samples from endogenously tagged Sdh4-GFP yeast. Spheroplast, SP; crude mitochondria, CM; soluble, S; elution, E (or IMM patch). Kar2, endoplasmic reticulum; Tom70, outer mitochondrial membrane (OMM); Vdac, OMM; Sdh4-GFP, SMALP target/IMM; Sdh2, IMM; Cit1, mitochondrial matrix. **g**, CoQ from subcellular fractions derived from SMALP isolation described in **f** for the indicated strains (mean ± SD, n = 3). **h**, Summary model depicting opposing roles for yeast UbiB family proteins in cellular distribution of CoQ. Significance calculated by a two-tailed Student's *t*-test; * = $p < 0.05$, ** = $p < 0.01$, *** = $p < 0.001$.

158 the Δ*cqd1*Δ*cqd2* strain recapitulated the respiratory growth deficiency of Δ*cqd1* (Fig.
159 4d). Total cellular CoQ levels remained unchanged (Extended Data Fig. 3b), again
160 suggesting these CoQ-related phenotypes are unrelated to CoQ biosynthesis. Similar to
161 Cqd1 (Fig. 3g), Cqd2 function was dependent on intact canonical PKL and UbiB-specific
162 residues (Fig. 4d, Extended Data Fig. 3c-e), suggesting that all three UbiB family
163 proteins in yeast are active phosphoryl transfer enzymes.

164 The analyses above, coupled with the submitochondrial location of Cqd1 and
165 Cqd2, suggest a model whereby these enzymes may reciprocally regulate the amount
166 of CoQ within the IMM. To test this directly, we used the amphipathic polymer styrene
167 maleic acid (SMA) to solubilize integral membrane proteins into detergent-free SMA
168 lipid particles (SMALPs)[20] from yeast harboring an endogenously-tagged subunit of
169 mitochondrial complex II (Sdh4-GFP). We reasoned that purifying lipid patches
170 containing Sdh4, which directly interacts with CoQ to facilitate succinate dehydrogenase
171 (Complex II) activity[21], would yield a suitable lipid microenvironment to measure IMM-
172 localized CoQ. After solubilization (Extended Data Fig. 3f), we isolated native IMM
173 patches that possessed Sdh4-GFP using a recombinantly purified His-tagged GFP
174 nanobody (Fig. 4e; Extended Data Fig. 3g-h). We show that purified Sdh4-GFP IMM
175 patches are largely void of extramitochondrial and outer mitochondrial membrane
176 (OMM) protein contamination (Fig. 4f), making this a reliable sample for assessing IMM
177 CoQ abundance.

178 We generated a panel of deletion strains in the Sdh4-GFP background to
179 investigate how loss of Cqd1 and Cqd2 impact CoQ abundance in this IMM
180 microenvironment. These yeast strains exhibited the same respiratory phenotypes as

the W303 background strains and had similar levels of whole-cell CoQ (Extended Data Fig. 3i-j). After solubilization and affinity enrichment (Extended Data Fig. 3k-l), Sdh4-GFP IMM patch lipids were extracted for targeted CoQ measurements. Consistent with our respiratory growth observations, Δ*cqd1* yeast had significantly lower levels of IMM patch CoQ. Conversely, the Δ*cqd2* yeast had elevated IMM patch CoQ, while Δ*cqd1*Δ*cqd2* yeast had levels similar to the parental strain (Fig. 4g). These data provide direct evidence of protein-dependent changes in CoQ distribution, corroborating our phenotypic observations. Taken together, our results suggest that Cqd1 and Cqd2 reciprocally regulate the levels of IMM CoQ and support a model wherein proper cellular CoQ distribution is dependent on the balance of their activities (Fig. 4h).

Discussion

Our work demonstrates that two previously uncharacterized UbiB family proteins influence the cellular distribution of mitochondria-derived CoQ. To our knowledge, Cqd1 and Cqd2 are the first proteins implicated in this process, which is essential for providing membranes throughout the cell with the CoQ necessary for enzymatic reactions and antioxidant defense. Further efforts are needed to establish how these proteins support CoQ distribution mechanistically; however, their similarity to Coq8 and the requirement for canonical PKL residues in their active sites suggests that Cqd1 and Cqd2 may couple ATPase activity to the selective extraction/deposition of CoQ from/to the IMM.

Once extracted from the IMM, we expect that subsequent steps would be required to deliver CoQ throughout the cell. The multimeric ER-mitochondrial encounter structure (ERMES) and mitochondrial contact site and cristae organizing system

(MICOS) complexes facilitate interorganellar lipid and metabolite transfer[22,23]. Recent work has revealed that CoQ biosynthetic machinery and MICOS subcomplexes often colocalize with ERMES[24-26], suggesting that these sites could serve as conduits for CoQ transport. Additionally, COQ9 is a lipid binding protein that likely delivers CoQ precursors to matrix enzymes[27], suggesting that other lipid binding proteins may exist to shuttle CoQ from mitochondria to other membranes. Our genetic screen has nominated several extramitochondrial and cytosolic proteins as promising leads for these processes.

Our investigations here focused on CoQ; however, it is possible that Cqd1 and Cqd2 (aka Mcp2) influence lipid transport and homeostasis more broadly. Previous work has identified an array of genetic interactions for Cqd1 and Cqd2 with lipid biosynthesis and homeostasis genes[19,28]. Moreover, Cqd2 was previously identified as a high-copy suppressor of a growth defect caused by loss of the ERMES subunit Mdm10[17]. More recently, three conserved Cqd2 active site residues were shown to mitigate rescue of Δ*mdm10* yeast growth[18], results that we confirm (Cqd2 K210R) and expand upon with six additional residue mutations.

Finally, UbiB family proteins are found across all domains of life[29]. UbiB homologs in plants (termed ABC1K proteins) are abundant, with 17 found in *Arabidopsis*[30]. Many of these ABC1K proteins are localized to plastoglobules—plastid-localized lipoprotein particles that contain various lipid-derived metabolites—and recent work suggests that ABC1K1 and ABC1K3 may affect the mobility and exchange of their subcellular plastoquinone-9 pools[31], suggesting UbiB proteins might function in quinone distribution across species. In humans, five UbiB proteins have been identified, ADCK1-

5. While COQ8A (ADCK3) and COQ8B (ADCK4) have established roles in CoQ biosynthesis and human disease[11,32,33], the biological roles of other ADCK proteins remain elusive. Genome-wide knockdown studies have implicated these uncharacterized *ADCK* genes in several cancer disease states[34-37]. As novel targets for human disease intervention, it will be important to determine if functional conservation exists between Cqd1 and Cqd2 and their putative human orthologs, ADCK2 and ADCK1/5, respectively. Recently, a crucial new role for extramitochondrial CoQ was identified in mitigating ferroptosis, a type of cell death stemming from a buildup of toxic lipid peroxides, suggesting that manipulating CoQ distribution could provide therapeutic benefits[38,39]. Notably, we have developed small-molecule modulators for Coq8[12] and COQ8A[40], indicating that UbiB proteins are promising druggable targets.

Collectively, our work to de-orphanize these poorly characterized mitochondrial proteins represents the first step in addressing enduring questions regarding endogenous cellular CoQ distribution and unlocking the therapeutic potential of manipulating this pathway.

Methods

Yeast Strains and Cultures

Unless otherwise described, *Saccharomyces cerevisiae* haploid W303 (MATa his3 leu2 met15 trp1 ura3) yeast were used. For SMA-derived lipid nanodisc work, endogenous GFP-tagged BY4741 (MATa his3Δ1 leu2Δ0 met15Δ0 ura3Δ0) yeast strains[41] were used. Yeast deletion strains were generated using standard homologous recombination or CRISPR-mediated methods. For homologous recombination, open reading frames

were replaced with the KanMX6, HygMX6, or NatMX6 cassette as previously described[42]. Cassette insertion was confirmed by a PCR assay and DNA sequencing. CRISPR-mediated deletions were performed as described in[43]. 20-mer guide sequences were designed with the ATUM CRISPR gRNA design tool (https://www.atum.bio/eCommerce/cas9/input) and cloned into pRCC-K, and 500 ng of the guide-inserted pRCC-K was used per yeast transformation. Donor DNA was 300 pmol of an 80-nt Ultramer consisting of 40 bp upstream and 40 bp downstream of the ORF (for scarless deletions) or ~6 µg of PCR-amplified Longtine cassette with flanking homology 40 bp upstream and 40 bp downstream of the ORF (for cassette-replacement deletions).

Synthetic complete (and dropout) media contained drop-out mix (US Biological), yeast nitrogen base (with ammonium sulfate and without amino acids) (US Biological), and the indicated carbon source. *p*ABA^{-} (and dropout) media contained Complete Supplement Mixture (Formedium), Yeast Nitrogen Base without amino acids and without *p*ABA (Formedium), and the indicated carbon source. All media were sterilized by filtration (0.22 µm pore size).

Yeast Growth Assay and Drop Assay

PUFA Growth Assays

To assay yeast growth in liquid media, individual colonies were used to inoculate synthetic complete (or synthetic complete dropout) media (2% glucose, w/v) starter cultures, which were incubated overnight (30 °C, 230 rpm). Yeast were diluted to

1.1×10^6 cells/mL in *p*ABA$^-$ (or *p*ABA$^-$ dropout) media (2% glucose, w/v) and incubated until early log phase (30 °C, 7-8 h, 230 rpm). Yeast were swapped into fresh *p*ABA$^-$ media (2% glucose, w/v) at an initial density of 5×10^6 cells/mL with indicated additives. The cultures were incubated (30 °C, 1140 rpm) in an Epoch2™ plate reader (BioTek®) in a sterile 96 well polystyrene round bottom microwell plate (Thermo) with a Breathe-Easy® cover seal (Diversified Biotech). Optical density readings (A_{600}) were obtained every 10 minutes, and growth rates were calculated with Gen5 v3.02.2 software (BioTek®), excluding timepoints from stationary phase.

Respiratory Growth Assays

Individual colonies of *S. cerevisiae* were used to inoculate synthetic complete media (2% glucose, w/v) starter cultures, which were incubated overnight (30 °C, 230 rpm). For transformed yeast strains, the corresponding Ura$^-$ media was used. Yeast were diluted to 1×10^6–1.33×10^6 cells/mL in *p*ABA$^-$ media (2% glucose, w/v) and incubated until early log phase (30 °C, 7-8 h, 230 rpm). Yeast were swapped into *p*ABA$^-$ media with glucose (0.1%, w/v) and glycerol (3%, w/v) at an initial density of 5×10^6 cells/mL with indicated additives. The cultures were incubated (30 °C, 1140 rpm) in an Epoch2 plate reader (BioTek) in a sterile 96 well polystyrene round bottom microwell plate (Thermo) with a Breathe-Easy cover seal (Diversified Biotech). Optical density readings (A_{600}) were obtained every 10 minutes, and growth rates were calculated with Gen5 v3.02.2 software (BioTek), excluding timepoints before the diauxic shift and during stationary phase growth.

297 *Drop Assays*

298 Individual colonies of yeast were used to inoculate *p*ABA-limited media (2% w/v
299 glucose, 100 nM *p*ABA) starter cultures, which were incubated overnight (30 °C,
300 230 rpm). Cells were spun down (21,000 x *g*, 2 min) and resuspended in water. Serial
301 dilutions of yeast (10^5, 10^4, 10^3, 10^2, or 10 cells) were dropped onto *p*ABA$^-$ media (2%
302 glucose and 1% EtOH, w/v) agar plates with indicated additives and incubated (30 °C,
303 2-3 d).

304

305 **Forward-genetic Screen**

306 Individual colonies of Δ*gpx1/2/3* yeast were used to inoculate YEPD starter cultures,
307 which were incubated overnight. 1.0×10^8 cells were pelleted, washed once with sterile
308 water, and resuspended in 2.5 mL of 100 mM sodium phosphate buffer, pH 7.0. Ethyl
309 methanesulfonate (EMS) (80 µL) was added, and cells were incubated (90 min, 30 °C,
310 230 rpm). Cells were washed thrice with sodium thiosulfate (5% w/v) to inactivate EMS.
311 Cells were resuspended in water, and 1.0×10^4 cells were plated on *p*ABA-limited (2%
312 w/v glucose, 100 nM *p*ABA) agar plates. After 3 days, cells were replica-plated onto
313 *p*ABA$^-$ (2% glucose, w/v) plates with 0 µM or 25 µM linolenic acid (C18:3, Sigma).
314 Colonies that grew on 25 µM linolenic acid were picked into YEPD overnight cultures
315 and struck on YEPD plates, and PUFA resistance phenotypes were confirmed with
316 plate reader growth assays. For mutant strains that grew in the presence of 25 µM
317 linolenic acid, genomic DNA was isolated with the MasterPure™ Yeast DNA Purification
318 Kit (Lucigen) and submitted to GENEWIZ for whole-genome sequencing. *S. cerevisiae*
319 genome assembly and variation calling were performed with SeqMan NGen 14 and

ArrayStar 14 (DNASTAR Lasergene suite). Variant D-Score predictions were obtained using the PROVEAN v1.1.3 web server (http://provean.jcvi.org/seq_submit.php).

Plasmid Cloning

Expression plasmids were cloned with standard restriction enzyme cloning methods. ORF specific primers were used to amplify Cqd1 (Ypl109c) and Cqd2 (Ylr253w) from W303 yeast genomic DNA. Amplicons were treated with DpnI to degrade genomic DNA and ligated into the digested p416 GPD plasmid (Addgene). Cloning products were then transformed into *E. coli* 10G chemically competent cells (Lucigen). Plasmids were isolated from transformants and Sanger sequencing was used to identify those containing the correct insertion.

Constructs containing Cqd1 and Cqd2 were digested with SalI and BamHI or HindIII to liberate the GPD promoter. Digested backbones were then combined with amplified endogenous promoter regions (1000 bases upstream for Cqd1, 500 bases upstream for Cqd2) and ligated to generate endogenous promoter vectors for Cqd1 and Cqd2.

Site-Directed Mutagenesis

Point mutants were constructed as described in the Q5® Site-Directed Mutagenesis Kit (New England Biolabs) and were confirmed via Sanger sequencing. Yeast were transformed as previously described[44] with plasmids encoding Cqd1 and Cqd2 variants

with their endogenous promoters and grown on uracil drop-out (Ura^-) synthetic media plates containing glucose (2%, w/v).

Homology Model Generation

Amino acid sequences of Cqd1 and Cqd2 were threaded through COQ8A apo crystal structure (PDB:4PED) via the online iTASSER webserver[45]. Superimposed homology models were visualized in the PyMOL Molecular Graphics System (Version 2.0, Schrödinger, LLC). Color schemes depicting protein domain organization were chosen according to previous work[15].

Subcellular Fractionation

Individual colonies of *S. cerevisiae* were used to inoculate synthetic complete media (2% glucose, w/v) starter cultures, which were incubated overnight (30 °C, 230 rpm). Yeast were diluted to 1.2×10^6 cells/mL in 50 mL *p*ABA^- media (2% glucose, w/v) and incubated until early log phase (30 °C, 12 h, 230 rpm). Yeast were swapped into 2 L of *p*ABA^- media with glucose (0.1%, w/v) and glycerol (3%, w/v) at an initial density of 5×10^4 cells/mL and incubated until early log phase (30 °C, 20 h, 230 rpm). $1x10^8$ cells were collected for whole-cell (WC) analyses. The remaining culture was pelleted by centrifugation (4,500 x g, 7 min) and weighed (5-6 g). Pellets were then fractionated using previously described methods[46]. To isolate crude mitochondria, samples were pelleted by centrifugation (15,000 x g, 10 min, 4 °C). Crude mitochondria were resuspended in SEM buffer (10 mM MOPS/KOH pH 7.2, 250 mM sucrose, 1 mM EDTA) containing 10 µg trypsin (sequencing grade, Promega) and rotated end-over-end

overnight (12 h, 4 °C) to disrupt proteinaceous organelle contact tethers[47]. Digested samples were pelleted by centrifugation (12,000 x g, 10 min, 4 °C) and the supernatant was collected. Pelleted material was resuspended in 900 µL SEM buffer containing 1 mM phenylmethylsulfonyl fluoride (SEM+PMSF) to deactivate trypsin. Resuspended material was pelleted (12,000 x g, 10 min, 4 °C) and the supernatant was collected. This was repeated once more and supernatant material was pooled (2.7 mL). To this, SEM buffer was added up to 10 mL before ultracentrifugation (106,000 x g, 1 h, 4 °C) to collect microsomes (non-mitochondrial fraction; NM). Pelleted crude mitochondria were resuspended in 700 µL SEM+PMSF and then added to a freshly prepared sucrose gradient (bottom to top: 1.5 mL 60% sucrose, 4 mL 32% sucrose, 1.5 mL 23% sucrose, and 1.5 mL 15% sucrose) for separation by ultracentrifugation (134,000 x g, 1 h, 4 °C). Enriched mitochondrial samples were recovered at the 32-60% interface and diluted with 30 mL SEM. Mitochondria were pelleted (15,000 x g, 10 min, 4 °C) and resuspended in fresh SEM (150 µL total). The protein concentration of all subcellular fractions (spheroplasts, SP; crude mitochondria, CM; non-mitochondrial fraction, NM; enriched mitochondria, M) was determined using the Pierce™ BCA Protein Assay Kit (Thermo) before Western blot (5 µg) analyses and lipid extractions.

GFP Nanobody

Recombinant Purification

pCA528-His-SUMO-GFP nanobody (GFPnb) constructs were transformed into RIPL competent *E. coli* cells for protein expression. GFPnb was overexpressed in *E. coli* by autoinduction overnight[48] (37 °C, 4 h; 20°C, 20 h). Cells were isolated by centrifugation

(4,500 x *g*, 12 min, RT), flash frozen in N_2(l) dropwise, and stored at -80 °C. For protein purification, cells were added to a Retsch® mixer mill MM 400 screw-top grinding jar pre-equilibrated with N_2(l). The cells were lysed by cryogenic grinding (-196 °C, 30 Hz, 120 s x 3). Ground cell pellet was collected and resuspended end-over-end for 1 h in lysis buffer (160 mM HEPES pH 7.5, 400 mM NaCl, 0.25 mM PMSF, 1 Roche cOmplete™ Protease Inhibitor Cocktail tablet, 500 U Benzonase® Nuclease) at 4 °C. The lysate was clarified by centrifugation (15,000 x *g*, 30 min, 4 °C). Clarified lysate was added to pre-equilibrated TALON® cobalt resin (Takara Bio) and incubated end-over-end for 1 h at 4 °C. TALON® resin was pelleted by centrifugation (700 x *g*, 2 min, 4 °C) and washed twice with equilibration buffer (160 mM HEPES pH 7.5, 400 mM NaCl, 0.25 mM PMSF) and twice with wash buffer (160 mM HEPES pH 7.5, 400 mM NaCl, 0.25 mM PMSF, 20 mM imidazole). His-tagged protein was eluted with elution buffer (160 mM HEPES (pH 7.5), 400 mM NaCl, 0.25 mM PMSF, 400 mM imidazole). The eluted protein was concentrated to ~600 µL with an Amicon® Ultra Centrifugal Filter (10 kDa MWCO) and exchanged into equilibration buffer. Concentrated protein elution was centrifuged (15,000 x *g*, 5 min, 4 °C) to pellet precipitate and filtered through a 0.22 µM syringe filter. Concentrated protein elution was separated via size exclusion chromatography on a HiLoad™ 16/600 Superdex™ 75 pg. Fractions from the size exclusion chromatography were analyzed by SDS-PAGE, and the fractions containing GFPnb were pooled and concentrated to ~1 mL. The concentration of GFPnb was determined by Bradford assay (Bio-Rad Protein Assay Kit II) and was diluted with equilibration buffer and glycerol to a final concentration of 20 mg/mL protein (160 mM HEPES pH 7.5, 400 mM NaCl, 10% glycerol). The final protein was aliquoted, flash

412 frozen in N_2(l) and stored at -80 °C. Fractions from the protein preparation were
413 analyzed by SDS-PAGE.
414
415 *Differential Scanning Fluorimetry*
416 The differential scanning fluorimetry method (thermal shift assay) was performed as
417 described previously[49]. Purified recombinant GFPnb was diluted to a final concentration
418 of 4 µM with DSF buffer (100 mM HEPES pH 7.5, 150mM NaCl) and 1:1250 SYPRO®
419 Orange Dye (Life Tech). Thermal shift data was collected with QuantStudio Real-Time
420 PCR v1.2 software and analyzed with Protein Thermal Shift v1.3 software.
421
422 **Native Nanodisc Isolation**
423 Individual colonies of *S. cerevisiae* (BY4741) were used to inoculate synthetic
424 complete media (2% glucose, w/v) starter cultures, which were incubated overnight (30
425 °C, 230 rpm). Yeast were diluted to 5×10^6 cells/mL in 50 mL *p*ABA$^-$ media (2% glucose,
426 w/v) and incubated until late log phase (30 °C, 16 h, 230 rpm). Yeast were swapped
427 into 2 L of *p*ABA$^-$ media with glucose (0.1%, w/v) and glycerol (3%, w/v) at an initial
428 density of 2.5×10^6 cells/mL and incubated until early log phase (30 °C, 16 h, 230 rpm).
429 Yeast cultures were pelleted by centrifugation (4,500 x g, 7 min) and weighed (2–3 g).
430 Pellets were then fractionated using previously described methods[46]. For preparative
431 scale affinity purification, crude mitochondria were resuspended in 50 µL BB7.4 (0.6 M
432 sorbitol, 20 mM HEPES-KOH pH 7.4), diluted in 950 µL ice cold BB7.S (20 mM HEPES-
433 KOH pH 7.4), vortexed for 10 sec (medium setting 8, Vortex Genie), and incubated on
434 ice for 30 minutes. Swollen mitochondria were then sonicated briefly (⅛'' tip, 20%

435 amplitude) for 2 - 5 second pulses with 60 seconds between pulses. Mitoplasts with
436 osmotically ruptured outer membranes were recovered by centrifugation at (20,000 × *g*,
437 10 min, 4 °C). After removing the supernatant, each pellet was resuspended with 1 mL
438 of Buffer B (20 mM HEPES-KOH pH 8.0, 200 mM NaCl) containing 2% (w/v) styrene
439 maleic acid copolymer (SMA, Polyscope SMALP® 25010P) by repeat pipetting and
440 rotated end-over-end (4 h, 4 °C). Soluble SMA extracts were separated from non-
441 extracted material by centrifugation at 21,000 × *g* for 10 min at 4 °C. Soluble material
442 was then were added to NTA nickel resin (400 µL slurry, Qiagen), which was pre-
443 charged (overnight at 4 °C, end-over-end) with recombinant His-tagged GFPnb (12.5
444 µL, 20 mg/mL). This mixture of soluble SMA extracts and charged nickel resin was
445 rotated end-over-end (24 h, 4 °C).
446
447 Nickel resin was pelleted by centrifugation (700 x *g*, 2 min, 4 °C) and the supernatant
448 fraction was carefully collected. Nickel resin was washed twice with Buffer B and twice
449 with 500 µL Wash Buffer [Buffer B containing 20 mM imidazole]. Native nanodiscs
450 bound to His-GFPnb were eluted with Buffer B containing 250 mM imidazole by rotating
451 end-over-end for 20 min at 4 °C. Due to the presence of GFP nanobody in the elution
452 samples, relative target abundance was determined by Western analysis and anti-GFP
453 band quantification. Protein concentrations of all other samples were quantified by
454 Pierce™ BCA Protein Assay Kit (Thermo).
455
456 **Lipid Extraction**
457 *$CHCl_3$:MeOH Extraction*

458 $1x10^8$ yeast cells were harvested by centrifugation (4,000 *g*, 5 min, 4 °C). The
459 supernatant was removed, and the cell pellet was flash frozen in N_2 (l) and stored at -80
460 C. (l) and stored at −80 °C. Frozen yeast pellets were thawed on ice and resuspended
461 in 100 µL cold water. To this, 100 µL of glass beads (0.5 mm; RPI) and CoQ_{10} internal
462 standard (10 µL, 10 µM) were added and bead beat (2 min, 4 °C). 900 µL extraction
463 solvent (1:1 $CHCl_3$/MeOH, 4 °C) was added and samples were vortexed briefly. To
464 complete phase separation, samples were acidified with 85 µL 6 M HCl (4 °C), vortexed
465 (2 x 30 s, 4 °C), and centrifuged (5,000 *g*, 2 min, 4 °C). The resulting aqueous layer
466 (top) was removed and 400 µL of the organic layer (bottom) was transferred to a clean
467 tube and dried under $Ar_{(g)}$. Dried organic matter (lipids) were reconstituted in
468 ACN/IPA/H_2O (65:30:5, v/v/v, 100 µL) by vortexing (2 x 30 s, RT) and transferred to an
469 amber vial (Sigma; QSertVial™, 12 x 32 mm, 0.3 mL) for LC–MS analysis.
470
471 *Petroleum Ether:MeOH Extraction*
472 For yeast whole-cell measurements, 1 $x10^8$ cells were collected by centrifugation (4,000
473 x *g*, 5 min) and layered with 100 µL of glass beads (0.5 mm; RPI). Whole-cell samples
474 and all other fractions were then suspended in ice-cold methanol (500 µL; with 1 µM
475 CoQ_8 internal standard) and vortexed (10 min, 4 °C). ~500 µL of petroleum ether was
476 added to extract lipids, and samples were vortexed (3 min, 4 °C) and centrifuged
477 (17,000 x *g*, 1 min) to separate phases. The petroleum ether (upper) layer was
478 collected, and the extraction was repeated with another round of petroleum ether (500
479 µL), vortexing (3 min, 4 °C), and centrifugation (17,000 x *g*, 1 min). The petroleum ether
480 layers were pooled and dried under argon. Lipids were resuspended in 2-propanol (15

μL) and transferred to amber glass vials (Sigma; QSertVial™, 12 x 32 mm, 0.3 mL). Sodium borohydride (15 μL of 10 mM in 2-propanol) was added to reduce quinones, and samples were vortexed briefly and incubated (5-10 min). Methanol (20 μL) was added to remove excess sodium borohydride, and samples were vortexed briefly and incubated (5-10 min). Samples were briefly flushed with nitrogen gas.

Lipidomic Analysis

Targeted LC-MS for Yeast CoQ_6 and $PPHB_6$

LC-MS analysis was performed on an Acquity CSH C18 column held at 50 °C (100 mm x 2.1 mm x 1.7 μm particle size; Waters) using a Vanquish Binary Pump (400 μL/min flow rate; Thermo Scientific). Mobile phase A consisted of 10 mM ammonium acetate and 250 μL/L acetic acid in ACN:H2O (70:30, v/v). Mobile phase B consisted of IPA:ACN (90:10, v/v) also with 10 mM ammonium acetate and 250 μL/L acetic acid. Mobile phase B was initially held at 50% for 1.5 min and then increased to 99% over 7.5 min and held there for 2 min. The column was equilibrated for 2.5 min before the next injection. 10 μL of each extract was injected by a Vanquish Split Sampler HT autosampler (Thermo Scientific) in a randomized order.

The LC system was coupled to a Q Exactive Orbitrap mass spectrometer (MS) through a heated electrospray ionization (HESI II) source (Thermo Scientific). Source conditions were as follow: HESI II and capillary temperature at 350 °C, sheath gas flow rate at 25 units, aux gas flow rate at 15 units, sweep gas flow rate at 5 units, spray voltage at +3.5

kV/-3.5 kV, and S-lens RF at 90.0 units. The MS was operated in a polarity switching mode acquiring positive and negative full MS and MS2 spectra (Top2) within the same injection. Acquisition parameters for full MS scans in both modes were 17,500 resolution, 1×10^6 automatic gain control (AGC) target, 100 ms ion accumulation time (max IT), and 200 to 1600 m/z scan range. MS2 scans in both modes were then performed at 17,500 resolution, 1×10^5 AGC target, 50 ms max IT, 1.0 m/z isolation window, stepped normalized collision energy (NCE) at 20, 30, 40, and a 10.0 s dynamic exclusion.

Parallel Reaction Monitoring (PRM) in positive polarity mode was utilized to monitor for two primary adducts, $[M+H]^+$ and $[M+NH^4]^+$, of each CoQ species. For CoQ_6, we targeted the mass to charge ratio of 592.449 and 609.475; for CoQ_8, 728.574 and 745.601; and for CoQ_{10}, 864.7 and 881.727. PRM MS settings were: Automatic gain control (AGC) target at $5x10^5$, Maximum IT at 100 ms, resolving power at 35,000, loop count at 2, isolation window at 3.0 *m/z,* and collision energy at 35. Another experiment performed in tandem with PRM used targeted single ion monitoring (t-SIM) in negative mode to determine the primary adduct, $[M-H]^-$, of CoQ intermediates. For $PPHB_6$, we targeted the mass to charge ratio of 544.908 and used the following t-SIM MS settings: AGC target at $5x10^5$, Maximum IT at 100 ms, and resolving power at 140,000 with an isolation window of 4.0 *m/z*.

Data Analysis

The resulting LC-MS data was manually processed using a custom TraceFinder 4.1 (Thermo Scientific) method using a mass precision of 4 and mass tolerance of 10 ppm to detect and identify the different species and adducts of CoQ_6 and CoQ_8 and intermediates.

Targeted HPLC-ECD for Yeast CoQ_6

For yeast whole-cell measurements, 5 x10^8 cells were collected by centrifugation (4,000 x *g*, 5 min) and layered with 100 µL of glass beads (0.5 mm; RPI). Lipids from whole-cell samples and other fractions were extracted according to the "*Petroleum Ether:MeOH Extraction*" section above. Samples were analyzed by reverse-phase high-pressure liquid chromatography with electrochemical detection (HPLC-ECD) using a C18 column (Thermo Scientific, Betasil C18, 100 x 2.1 mm, particle size 3 µm) at a flow rate of 0.3 mL/min with a mobile phase of 75% methanol, 20% 2-propanol, and 5% ammonium acetate (1 M, pH 4.4). After separation on the column, the $NaBH_4$-reduced quinones were quantified on ECD detector (Thermo Scientific ECD3000-RS) equipped with 6020RS omni Coulometric Guarding Cell "E1", and 6011RS ultra Analytical Cell "E2" and "E3". To prevent premature quinone oxidation, the E1 guarding electrode was set to −200 mV. Measurements were made using the analytical E2 electrode operating at 600 mV after complete oxidation of the quinone sample and E3 electrode (600 mV) was used to ensure that total signal was recorded on the E2 cell. For each experiment, a CoQ_6 standard in 2-propanol was also prepared with sodium borohydride and methanol treatment, and different volumes were injected to make a standard curve. Quinones

were quantified by integrating respective peaks using the Chromeleon 7.2.10 software (Thermo) and normalized to CoQ_8 internal standard.

Antibodies and Western Blots

Antibodies

Primary antibodies used in this study include anti-Kar2 (SCBT sc-33630, 1:5000; RRID: AB_672118), anti-Cit1[50] (Biomatik, 1:4000), anti-β-actin (Abcam ab8224, 1:1000; RRID: AB_449644), anti-Tom70[51] (1:1000, a gift from Nora Vogtle, University of Freiburg), anti-Vdac (Abcam ab110326, 1:2000; RRID: AB_10865182); anti-GFP (SCBT sc-9996, 1:1000; RRID: AB_627695), anti-Sdh2[52] (1:5000, a gift from Oleh Khalimonchuk, University of Nebraska). Secondary antibodies include goat anti-mouse (LI-COR 926-32210, 1:15000; RRID: AB_621842) and goat anti-rabbit (LI-COR 926-32211, 1:15000; RRID: AB_621843).

SMA Solubility Western Blot

Mitoplasts were recovered and solubilized in styrene maleic acid containing buffer as described above in "*Native Nanodisc Isolation.*" To determine the extent of GFP target solubilization, equal amounts of "input" (IP) and soluble supernatant (S) were obtained, along with the total pellet (insoluble, IS). 75 µL of the input sample was collected immediately after SMA solubilization. After separating soluble SMA extracts from non-extracted material via centrifugation (21,000 × *g*, 10 min, 4 °C), the supernatant was transferred to a clean tube for an additional 5 minute spin. 75 µL of soluble sample was then transferred to a new tube. The resulting pellet was washed with 1 mL of Buffer B

and centrifuged (21,000 × *g* for 5 min at 4 °C). The resulting supernatant was aspirated and 75 µL of Buffer B was added to the insoluble (IS) fraction. From each sample, proteins were extracted by standard chloroform-methanol procedures. Precipitated protein was reconstituted in 75 µL 0.1 M NaOH. 25 µL 4X LDS sample buffer containing beta-mercaptoethanol (BME) was added and samples were incubated (95 °C, ~10 min). Proteins were analyzed with 4–12% Novex NuPAGE Bis-Tris SDS-PAGE (Invitrogen) gels (1 h, 150 V). The gel was transferred to PVDF membrane at 100 V for 1 h with transfer buffer (192 mM glycine, 25 mM Tris, 20% methanol [v/v]). The membrane was blocked with 5% nonfat dry milk (NFDM) in TBST (20 mM Tris pH 7.4, 150 mM NaCl, 0.05% Tween 20 [v/v]) (1 h with agitation). Antibodies were diluted in 1% NFDM in TBST and incubated with the PVDF (overnight, 4 °C with agitation). The PVDF was washed three times in TBST and the secondary antibodies were diluted 1:15,000 in 1% NFDM in TBST (1.5 h, r.t.). The membrane was washed three times in TBST and imaged on a LI-COR Odyessey CLx using Image Studio v5.2 software.

SMALP Fractionation Western Blot

Fractions described above in "*Native Nanodisc Isolation*" and "*SMA Solubility Western Blot*" were collected and used for western blot analysis. 4 µg of spheroplasts (SP) and crude mitochondria (CM) were loaded, along with equal volumes of extracted soluble (S) and final elution (E) samples. Western blots were performed as described above.

Statistical Analysis

All experiments were performed in at least biological triplicate, unless stated otherwise. In all cases, "mean" refers to arithmetic mean, and "SD" refers to sample standard deviation. Statistical analyses were performed using Microsoft Excel. *p*-values were calculated using an unpaired, two-tailed, Student's *t*-test. In all cases, *n* represents independent replicates of an experiment.

Reporting Summary

Further information on research design is available in the Nature Research Reporting Summary linked to this article.

Data availability

Next generation sequencing data (Fig. 2, Extended Data Fig 1) have been deposited to NCBI SRA (BioProject ID PRJNA679831; SRA accession SRP293543). Additional source data for Fig. 1-4 and Extended Data 1-3 are provided with the paper. All other data supporting the finding of this study are available from the corresponding authors on reasonable request.

612 ## References

613 1. Hatefi, Y., Haavik, A.G., Fowler, L.R. & Griffiths, D.E. Studies on the electron
614 transfer system. XLII. Reconstitution of the electron transfer system. *J Biol Chem*
615 **237**, 2661-2669 (1962).
616 2. Frerman, F.E. Acyl-CoA dehydrogenases, electron transfer flavoprotein and
617 electron transfer flavoprotein dehydrogenase. *Biochem Soc Trans* **16**, 416-418
618 (1988).
619 3. Jones, M.E. Pyrimidine nucleotide biosynthesis in animals: genes, enzymes, and
620 regulation of UMP biosynthesis. *Annu Rev Biochem* **49**, 253-279 (1980).
621 4. Bentinger, M., Brismar, K. & Dallner, G. The antioxidant role of coenzyme Q.
622 *Mitochondrion* **7 Suppl**, S41-50 (2007).
623 5. Do, T.Q., Schultz, J.R. & Clarke, C.F. Enhanced sensitivity of ubiquinone-
624 deficient mutants of Saccharomyces cerevisiae to products of autoxidized
625 polyunsaturated fatty acids. *Proc Natl Acad Sci U S A* **93**, 7534-7539 (1996).
626 6. Avery, A.M. & Avery, S.V. Saccharomyces cerevisiae expresses three
627 phospholipid hydroperoxide glutathione peroxidases. *J Biol Chem* **276**, 33730-
628 33735 (2001).
629 7. Choi, Y., Sims, G.E., Murphy, S., Miller, J.R. & Chan, A.P. Predicting the
630 functional effect of amino acid substitutions and indels. *PLoS One* **7**, e46688
631 (2012).
632 8. Tauche, A., Krause-Buchholz, U. & Rodel, G. Ubiquinone biosynthesis in
633 Saccharomyces cerevisiae: the molecular organization of O-methylase Coq3p
634 depends on Abc1p/Coq8p. *FEMS Yeast Res* **8**, 1263-1275 (2008).

9. Vogtle, F.N. *et al.* Landscape of submitochondrial protein distribution. *Nat Commun* **8**, 290 (2017).

10. Rhee, H.W. *et al.* Proteomic mapping of mitochondria in living cells via spatially restricted enzymatic tagging. *Science* **339**, 1328-1331 (2013).

11. Stefely, J.A. *et al.* Cerebellar Ataxia and Coenzyme Q Deficiency through Loss of Unorthodox Kinase Activity. *Mol Cell* **63**, 608-620 (2016).

12. Reidenbach, A.G. *et al.* Conserved Lipid and Small-Molecule Modulation of COQ8 Reveals Regulation of the Ancient Kinase-like UbiB Family. *Cell Chem Biol* **25**, 154-165 e111 (2018).

13. Morgenstern, M. *et al.* Definition of a High-Confidence Mitochondrial Proteome at Quantitative Scale. *Cell Rep* **19**, 2836-2852 (2017).

14. Vazquez-Fonseca, L. *et al.* ADCK2 Haploinsufficiency Reduces Mitochondrial Lipid Oxidation and Causes Myopathy Associated with CoQ Deficiency. *J Clin Med* **8** (2019).

15. Stefely, J.A. *et al.* Mitochondrial ADCK3 employs an atypical protein kinase-like fold to enable coenzyme Q biosynthesis. *Mol Cell* **57**, 83-94 (2015).

16. Kannan, N., Taylor, S.S., Zhai, Y., Venter, J.C. & Manning, G. Structural and functional diversity of the microbial kinome. *PLoS Biol* **5**, e17 (2007).

17. Tan, T., Ozbalci, C., Brugger, B., Rapaport, D. & Dimmer, K.S. Mcp1 and Mcp2, two novel proteins involved in mitochondrial lipid homeostasis. *J Cell Sci* **126**, 3563-3574 (2013).

18. Odendall, F. *et al.* The mitochondrial intermembrane space-facing proteins Mcp2 and Tgl2 are involved in yeast lipid metabolism. *Mol Biol Cell* **30**, 2681-2694 (2019).

19. Costanzo, M. *et al.* A global genetic interaction network maps a wiring diagram of cellular function. *Science* **353** (2016).

20. Lee, S.C. *et al.* A method for detergent-free isolation of membrane proteins in their local lipid environment. *Nat Protoc* **11**, 1149-1162 (2016).

21. Oyedotun, K.S. & Lemire, B.D. The Quinone-binding sites of the Saccharomyces cerevisiae succinate-ubiquinone oxidoreductase. *J Biol Chem* **276**, 16936-16943 (2001).

22. Murley, A. & Nunnari, J. The Emerging Network of Mitochondria-Organelle Contacts. *Mol Cell* **61**, 648-653 (2016).

23. Tamura, Y., Kawano, S. & Endo, T. Organelle contact zones as sites for lipid transfer. *J Biochem* **165**, 115-123 (2019).

24. Subramanian, K. *et al.* Coenzyme Q biosynthetic proteins assemble in a substrate-dependent manner into domains at ER-mitochondria contacts. *J Cell Biol* **218**, 1353-1369 (2019).

25. Eisenberg-Bord, M. *et al.* The Endoplasmic Reticulum-Mitochondria Encounter Structure Complex Coordinates Coenzyme Q Biosynthesis. *Contact (Thousand Oaks)* **2**, 2515256418825409 (2019).

26. Tirrell, P.S., Nguyen, K.N., Luby-Phelps, K. & Friedman, J.R. MICOS subcomplexes assemble independently on the mitochondrial inner membrane in proximity to ER contact sites. *J Cell Biol* **219** (2020).

679 27. Lohman, D.C. *et al.* An Isoprene Lipid-Binding Protein Promotes Eukaryotic
680 Coenzyme Q Biosynthesis. *Mol Cell* **73**, 763-774 e710 (2019).
681 28. Hoppins, S. *et al.* A mitochondrial-focused genetic interaction map reveals a
682 scaffold-like complex required for inner membrane organization in mitochondria.
683 *J Cell Biol* **195**, 323-340 (2011).
684 29. Leonard, C.J., Aravind, L. & Koonin, E.V. Novel families of putative protein
685 kinases in bacteria and archaea: evolution of the "eukaryotic" protein kinase
686 superfamily. *Genome Res* **8**, 1038-1047 (1998).
687 30. Lundquist, P.K., Davis, J.I. & van Wijk, K.J. ABC1K atypical kinases in plants:
688 filling the organellar kinase void. *Trends Plant Sci* **17**, 546-555 (2012).
689 31. Pralon, T. *et al.* Mutation of the Atypical Kinase ABC1K3 Partially Rescues the
690 PROTON GRADIENT REGULATION 6 Phenotype in Arabidopsis thaliana. *Front*
691 *Plant Sci* **11**, 337 (2020).
692 32. Ashraf, S. *et al.* ADCK4 mutations promote steroid-resistant nephrotic syndrome
693 through CoQ10 biosynthesis disruption. *J Clin Invest* **123**, 5179-5189 (2013).
694 33. Lagier-Tourenne, C. *et al.* ADCK3, an ancestral kinase, is mutated in a form of
695 recessive ataxia associated with coenzyme Q10 deficiency. *Am J Hum Genet* **82**,
696 661-672 (2008).
697 34. Wiedemeyer, W.R. *et al.* Pattern of retinoblastoma pathway inactivation dictates
698 response to CDK4/6 inhibition in GBM. *Proc Natl Acad Sci U S A* **107**, 11501-
699 11506 (2010).
700 35. Brough, R. *et al.* Functional viability profiles of breast cancer. *Cancer Discov* **1**,
701 260-273 (2011).

36. Simpson, K.J. *et al.* Identification of genes that regulate epithelial cell migration using an siRNA screening approach. *Nat Cell Biol* **10**, 1027-1038 (2008).

37. Qiu, M. *et al.* aarF domain containing kinase 5 gene promotes invasion and migration of lung cancer cells through ADCK5-SOX9-PTTG1 pathway. *Exp Cell Res* **392**, 112002 (2020).

38. Bersuker, K. *et al.* The CoQ oxidoreductase FSP1 acts parallel to GPX4 to inhibit ferroptosis. *Nature* **575**, 688-692 (2019).

39. Doll, S. *et al.* FSP1 is a glutathione-independent ferroptosis suppressor. *Nature* **575**, 693-698 (2019).

40. Asquith, C.R.M., Murray, N.H. & Pagliarini, D.J. ADCK3/COQ8A: the choice target of the UbiB protein kinase-like family. *Nat Rev Drug Discov* **18**, 815 (2019).

41. Huh, W.K. *et al.* Global analysis of protein localization in budding yeast. *Nature* **425**, 686-691 (2003).

42. Baudin, A., Ozier-Kalogeropoulos, O., Denouel, A., Lacroute, F. & Cullin, C. A simple and efficient method for direct gene deletion in Saccharomyces cerevisiae. *Nucleic Acids Res* **21**, 3329-3330 (1993).

43. Generoso, W.C., Gottardi, M., Oreb, M. & Boles, E. Simplified CRISPR-Cas genome editing for Saccharomyces cerevisiae. *J Microbiol Methods* **127**, 203-205 (2016).

44. Gietz, R.D. & Woods, R.A. Transformation of yeast by lithium acetate/single-stranded carrier DNA/polyethylene glycol method. *Methods Enzymol* **350**, 87-96 (2002).

724 45. Yang, J. *et al.* The I-TASSER Suite: protein structure and function prediction. *Nat*
725 *Methods* **12**, 7-8 (2015).
726 46. Meisinger, C., Pfanner, N. & Truscott, K.N. Isolation of yeast mitochondria.
727 *Methods Mol Biol* **313**, 33-39 (2006).
728 47. Forner, F., Arriaga, E.A. & Mann, M. Mild protease treatment as a small-scale
729 biochemical method for mitochondria purification and proteomic mapping of
730 cytoplasm-exposed mitochondrial proteins. *J Proteome Res* **5**, 3277-3287
731 (2006).
732 48. Fox, B.G. & Blommel, P.G. Autoinduction of protein expression. *Curr Protoc*
733 *Protein Sci* **Chapter 5**, Unit 5 23 (2009).
734 49. Niesen, F.H., Berglund, H. & Vedadi, M. The use of differential scanning
735 fluorimetry to detect ligand interactions that promote protein stability. *Nat Protoc*
736 **2**, 2212-2221 (2007).
737 50. Guo, X. *et al.* Ptc7p Dephosphorylates Select Mitochondrial Proteins to Enhance
738 Metabolic Function. *Cell Rep* **18**, 307-313 (2017).
739 51. Vogtle, F.N. *et al.* Mutations in PMPCB Encoding the Catalytic Subunit of the
740 Mitochondrial Presequence Protease Cause Neurodegeneration in Early
741 Childhood. *Am J Hum Genet* **102**, 557-573 (2018).
742 52. Bohovych, I. *et al.* Metalloprotease OMA1 Fine-tunes Mitochondrial Bioenergetic
743 Function and Respiratory Supercomplex Stability. *Sci Rep* **5**, 13989 (2015).
744
745

Acknowledgements

We thank Steven Claypool for consultation on SMALP generation, Adam Frost for providing the plasmid containing GFP nanobody, Nora Vogtle and Oleh Khalimonchuk for providing mitochondrial antibodies, Jared Rutter and Jodi Nunnari for providing the parental yeast strains used in our studies, Matt Stefely for assistance with figure generation, and current and former members of the Pagliarini Laboratory for their feedback. This work was supported by NIH R35GM131795 and R01 GM112057 (to D.J.P.), NIH T32DK007665, William H. Peterson Fellowship, Washburn Wharton Fellowship, and University of Wisconsin Biochemistry Funding (to Z.A.K.), a National Science Foundation Graduate Research Fellowship DGE-1747503 (to K.P.R.), and P41GM108538 (to J.J.C. and D.J.P.).

Author information

These authors contributed equally: Zachary A. Kemmerer, Kyle P. Robinson.

Affiliations

Morgridge Institute for Research, Madison, WI, USA.

Zachary A. Kemmerer, Kyle P. Robinson, Jonathan M. Schmitz, Adam Jochem, and David J. Pagliarini

Department of Biochemistry, University of Wisconsin-Madison, Madison, WI, USA.

Zachary A. Kemmerer, Kyle P. Robinson, Jonathan M. Schmitz, Adam Jochem, and David J. Pagliarini

Genome Center of Wisconsin, Madison, Wisconsin, USA.

Joshua J. Coon

Department of Chemistry, University of Wisconsin-Madison, Madison, WI, USA.

Brett R. Paulson, Paul D. Hutchins, and Joshua J. Coon

Department of Biomolecular Chemistry, University of Wisconsin-Madison, Madison, WI, USA.

Joshua J. Coon

Departments of Cell Biology and Physiology; Biochemistry and Molecular Biophysics; and Genetics, Washington University School of Medicine, St. Louis, MO, USA

David J. Pagliarini

Contributions

Z.A.K., K.P.R., and D.J.P. conceived of the project and its design. Z.A.K. and K.P.R. conducted experiments and performed data analysis. J.M.S. purified and characterized GFP nanobody. B.R.P. and P.D.H. performed and analyzed mass spectrometry experiments. A.J. contributed to new reagents (cloning). All authors edited the manuscript. Z.A.K., K.P.R., and D.J.P. wrote the manuscript. D.J.P. supervised the project.

Corresponding Author

Correspondence and requests for materials should be addressed to D.J.P. (pagliarini@wustl.edu).

Ethics declaration

Competing interests

J.J.C. is a consultant for Thermo Fisher Scientific.

Extended data

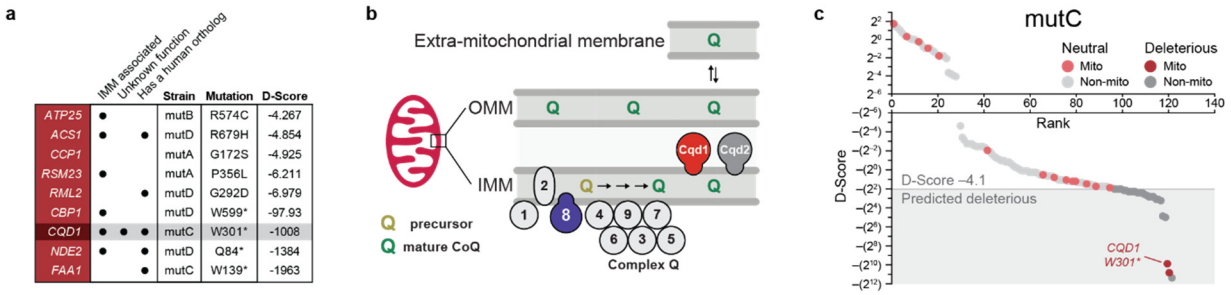

Extended Data Fig. 1 Genome-wide screen for CoQ trafficking genes identifies uncharacterized UbiB protein Cqd1. a, Criteria for nine mitochondrial candidates used to nominate genes for additional investigation. Submitochondrial localization was confirmed by comparison to previous submitochondrial profiling datasets[9], while protein function and human ortholog criteria were determined with existing database mining (UniProt and PhylomeDB, respectively). **b,** Schematic showing the submitochondrial localization of UbiB family proteins Coq8 (purple), Cqd1 (red), and Cqd2 (gray). Coq8 is essential for CoQ biosynthesis in concert with other Coq proteins (Coq1-9). **c**, Non-synonymous mutations identified using whole-genome sequencing for strain mutC were analyzed with PROVEAN to filter for likely deleterious changes (D-score ≤ -4.1, shaded box). Gray, all genes; red, mitochondrial genes. Light, predicted neutral; dark, predicted deleterious.

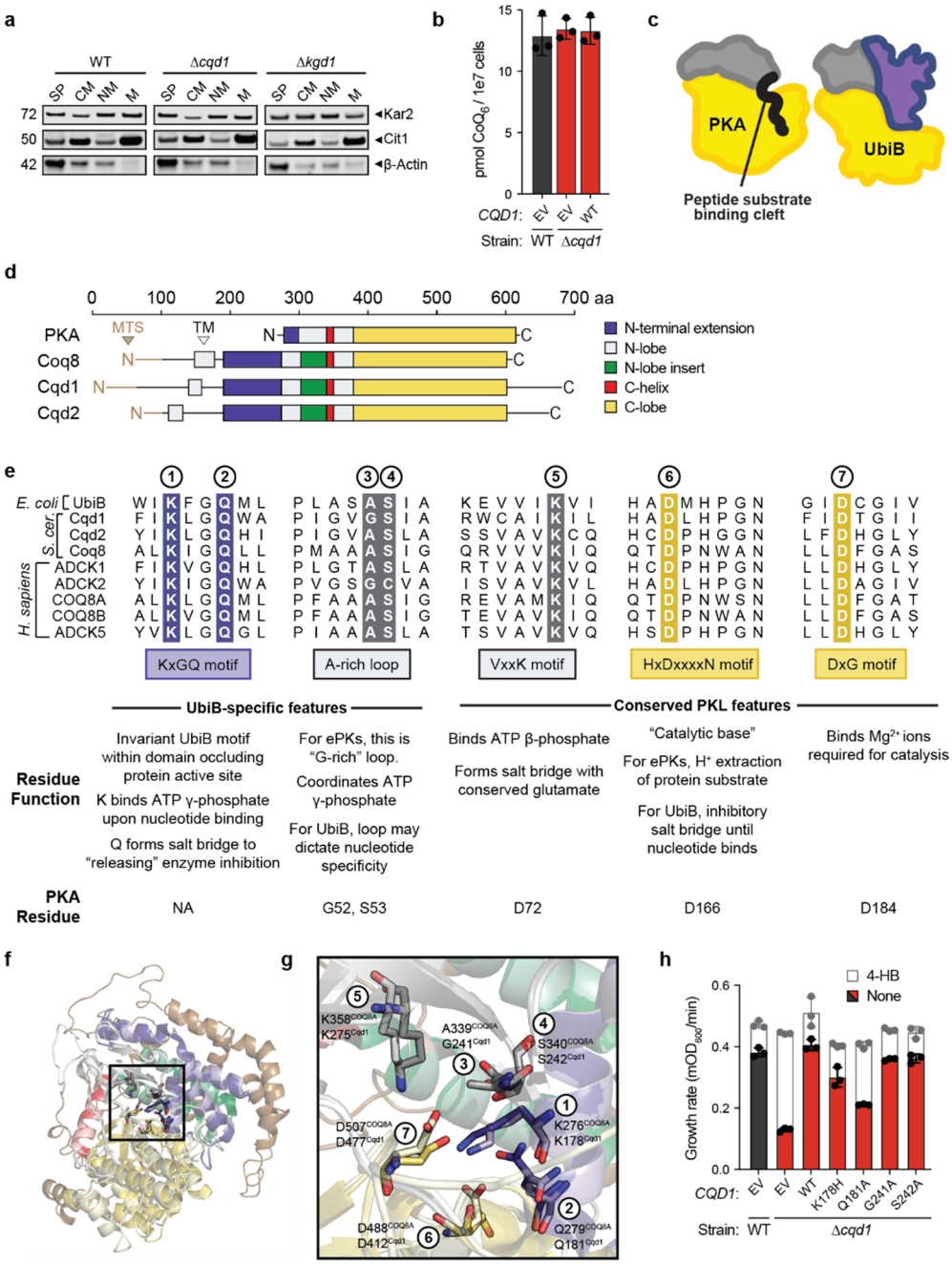

805

806 **Extended Data Fig. 2 Cqd1 influences cellular CoQ distribution. a**, Western blot of subcellular samples derived from fractionated WT, Δ*cqd1*, and Δ*kgd1* yeast. Spheroplast, SP; crude mitochondria, CM; non-mitochondrial fraction, NM; enriched mitochondria, M. Kar2, endoplasmic reticulum; Cit1, mitochondria; β-actin, cytoplasm. **b**, Total CoQ from WT and Δ*cqd1* yeast transformed with the indicated plasmids and grown in Ura–, *p*ABA– media containing 0.1% (w/v) glucose and 3% (w/v) glycerol (mean ± SD, n = 3). **c**, Cartoon of canonical protein kinase A (PKA; 1ATP) and human COQ8A (4PED) showing protein domain organization. Protein kinases often contain a β-sheet rich N-terminal domain (gray) and a helical C-terminal domain (yellow). COQ8A contains a unique N-terminal extension (purple) containing the invariant UbiB-specific 'KxGQ' motif. **d**, Domain alignment of PKA and yeast UbiB proteins. Mitochondrial targeting sequence, MTS; transmembrane domain, TM. **e**, UbiB family sequence alignment of UbiB-specific and conserved protein kinase-like (PKL) features. Residue functions within the canonical protein kinase or UbiB architecture are described below. The three conserved PKL residues shown are essential for phosphoryl transfer activity. **f**, Homology model for Cqd1 (light) aligned with COQ8A (4PED, dark). The model was threaded using I-TASSER[45] and COQ8A structure to guide modeling. Boxed and outlined in black are residues described in **g**, and unmodeled regions are colored in brown. **i**, Zoomed in view of conserved PKL and UbiB-specific residues. **h**, Growth rate of WT and Δ*cqd1* yeast transformed with the indicated plasmids (EV, *CQD1* or *CQD1* point mutants*)* and grown in Ura–, *p*ABA– media containing 0.1% (w/v) glucose and 3% (w/v) glycerol (mean ± SD, n = 3). Yeast were treated with 0 (colored bars) or 1 μM 4-HB (white bars, superimposed) to determine rescue of respiratory growth.

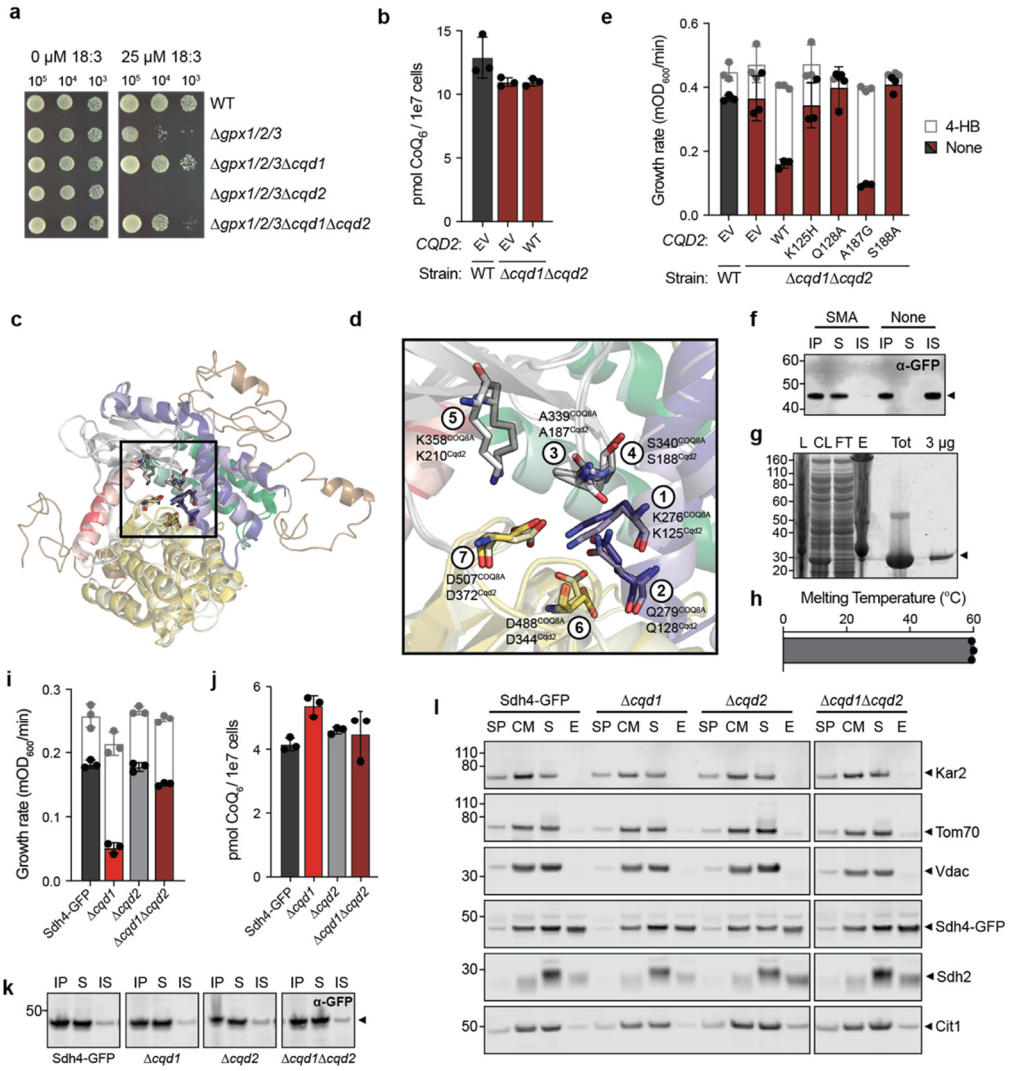

807

Extended Data Fig. 3 Cqd2 function opposes Cqd1 control of CoQ distribution.

a, Serial dilution drop assay of indicated yeast strains grown for 3 days on solid *p*ABA– medium containing 2% (w/v) glucose, 0.5% (w/v) ethanol (EtOH), and 0-25 μM 18:3. **b**, Total CoQ from WT and Δ*cqd1*Δ*cqd2* yeast transformed with EV or endogenous *CQD2* and grown in Ura–, *p*ABA– media containing 0.1% (w/v) glucose and 3% (w/v) glycerol (mean ± SD, n = 3). **c**, Homology model for Cqd2 (light) aligned with COQ8A (4PED, dark). The model was threaded using I-TASSER[45] and COQ8A structure to guide modeling. Boxed and outlined in black are residues described previously (**Extended Data Fig. 2f**) and unmodeled regions are colored in brown. **d**, Zoomed in view of conserved PKL and UbiB-specific residues described previously. **e**, Growth rate of WT and Δ*cqd1*Δ*cqd2* yeast transformed with the indicated plasmids and grown in Ura–, *p*ABA– media containing 0.1% (w/v) glucose and 3% (w/v) glycerol (mean ± SD, n = 3). Yeast were treated with 0 (colored bars) or 1 μM 4-HB (white bars, superimposed) to determine recapitulation of respiratory growth defect. **f**, Western blot to determine solubility of Sdh4-GFP target in the presence and absence of 2% (w/v) SMA. Input, IP; soluble, S; insoluble, IS. **g**, Recombinant purification of His-tagged GFP nanobody (GFPnb) via nickel resin enrichment and size-exclusion isolation. Lysate, L; clarified lysate, CL; flow-through, FT; elution, E; size-exclusion chromatography, SEC. **h**, Differential scanning fluorimetry of recombinant GFPnb to determine protein melting temperature. **i**, Growth rate of Sdh4-GFP yeast and indicated deletion strains assayed in *p*ABA– media containing 0.1% (w/v) glucose and 3% (w/v) glycerol and treated with 0 (colored bars) or 1 μM 4-HB (white bars, superimposed) (mean ± SD, n = 3). **j**, Total CoQ from yeast strains described in **i. k**, Western blot to determine solubility of Sdh4-GFP target during SMALP preparation from the indicated yeast strains. Input, IP; soluble, S; insoluble, IS. **l**, Western blot of SMALP isolation samples derived from the indicated yeast. Spheroplast, SP; crude mitochondria, CM; soluble, S; elution, elution, E (or IMM patch). Kar2, endoplasmic reticulum; Tom70, OMM; Vdac, OMM; Sdh4-GFP, SMALP target/IMM; Sdh2, IMM; Cit1, mitochondrial matrix.